Accepted Manuscript

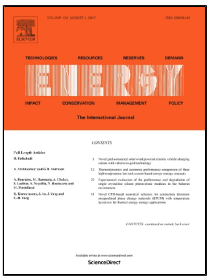

Multi-Objective Optimization of Nanofluid Flow in Double Tube Heat Exchangers for Applications in Energy Systems

Mohammad Hemmat Esfe, Hadi Hajmohammad, Davood Toghraie, Hadi Rostamian, Omid Mahian, Somchai Wongwises

PII:	S0360-5442(17)31101-5
DOI:	10.1016/j.energy.2017.06.104
Reference:	EGY 11112
To appear in:	*Energy*
Received Date:	13 June 2016
Revised Date:	26 May 2017
Accepted Date:	18 June 2017

Please cite this article as: Mohammad Hemmat Esfe, Hadi Hajmohammad, Davood Toghraie, Hadi Rostamian, Omid Mahian, Somchai Wongwises, Multi-Objective Optimization of Nanofluid Flow in Double Tube Heat Exchangers for Applications in Energy Systems, *Energy* (2017), doi: 10.1016/j.energy.2017.06.104

.

Multi-Objective Optimization of Nanofluid Flow in Double Tube Heat Exchangers for Applications in Energy Systems

Mohammad Hemmat Esfe[1], Hadi Hajmohammad[1], Davood Toghraie[1], Hadi Rostamian[1], Omid Mahian[2*], Somchai Wongwises[3]

[1]Department of Mechanical Engineering, Khomeinishahr Branch, Islamic Azad University, Isfahan, Iran

[2] Renewable Energies, Magnetism and Nanotechnology Lab., Faculty of Science, Ferdowsi University of Mashhad, Mashhad, Iran

[3]Fluid Mechanics, Thermal Engineering and Multiphase Flow Research Laboratory (FUTURE Lab.), Department of Mechanical Engineering, King Mongkut's University of Technology Thonburi, Bangmod, Bangkok 10140, Thailand

*Corresponding author E-Mail:omid.mahian@gmail.com

Abstract

The optimization of MgO-water nanofluids in order to reduce the cost and increase the heat transfer coefficient is investigated in this study. At first, the heat transfer coefficient is obtained at various values of solid volume fractions, diameters of nanoparticles, and Reynolds numbers based on empirical data. The cost amount is also determined in terms of solid volume fractions and diameters of nanoparticles. Then, the heat transfer coefficient function and the cost function are attained via RSM (Response Surface Method) and with a regression coefficient of over 0.997. The optimization is performed by the non-dominated sorting genetic algorithm which has a significant capability of achieving optimal response. Finally, the Pareto front, the optimal heat transfer coefficient, and their corresponding minimum cost have been obtained. An appropriate correlation is also provided to achieve the optimal model of the minimum cost in terms of the maximum heat transfer coefficient. Optimization results have shown that, compared to the first optimization, the cost has decreased about 38% in the best case.

Keywords:

Multi-objective optimization; Response surface method; Nanofluid; Heat transfer coefficient

1. Introduction

By the invention of nanofluids, many researchers have devoted their studies to this subject. The application of nanofluids in energy systems is developing quickly.

Heat transfer enhancement and the need to more impact energy systems are just two main reasons that researchers have been encouraged to continue the investigation in this area. In an article, Eastman et al. [1] reported the thermal conductivity enhancement of 40% for metal nanofluids of Cu-EG at a solid volume fraction of 0.3%. Choi et al. [2] have also recorded an enhancement of 160% for α–olefin oil nanofluids containing CNT nanoparticles.

As stated, different properties of nanofluids are investigated. Using nanofluids aims at increasing the rate of heat transfer in the cooling equipment. So, the convective heat transfer coefficient is one of the most important properties studied in nanofluids' issue.

Pakdaman et al. [3] have investigated thermophysical properties and overall efficiency of MWCNT/heat transfer oil nanofluids within the vertical helically coiled tubes. It was reported that the performance index of system reaches 5.1 which shows high potential of nanofluids for heat transfer enhancement. In an experimental study on nanofluids, Razi et al. [4] have surveyed the pressure drop and thermal properties of CuO-oil nanofluids, and probed nanofluid's efficiency within flattened tubes at constant heat flux. The heat transfer, pressure drop and efficiency of MgO, MWCNT and DWCNT nanofluids have been experimentally measured in separate studies by Esfe et al. [5-7]. Due to the extent of subjects in nanofluids' area, the data derived from experiments should be processed in order to make nanofluids as practical as possible. Recently, some researchers have managed to develop this method, and they processed and modeled the experimental data relating to the thermal conductivity [8-13] and viscosity [14-17] by means of artificial neural networks. Some researches were also aimed at discovering optimal modes of nanofluids application. For example, Yang et al. [18] optimized the turbulent flow of nanofluids in a rectangular rib-grooved channel using RSM-GA algorithm, Boyaghchi et al. [19] optimized the heat transfer, pressure drop and efficiency in micro-channels, Safikhani et al.[20] considered the optimization of heat transfer and pressure drop in flat tubes by ANN NSGA II algorithm, Halelfadl et al. [21] optimized the thermal performance and pressure drop in microchannel heat sinks by NSGA-II algorithm and some other studies [22-23] can be cited in this section.

The new approach addressed in this paper, which has not been addressed in the field of nanofluids yet, is the optimization of heat transfer coefficient of nanofluids as compared to their cost by NSGA-II method using response surface approximation, at different solid volume fractions and sizes of nanoparticles. For this purpose, the heat transfer coefficient data of MgO-water nanofluids

is extracted from Esfe et al. [24]. Then, to designate the objective functions, the heat transfer coefficient of nanofluid is determined by experiment in terms of various quantities of solid volume fraction, nanoparticle's diameter, and Reynolds number. Using the heat transfer coefficient and the cost in terms of intended variables, the correlation of heat transfer coefficient and the cost is attained. By considering obtained correlations of the optimization algorithm, results of the Pareto front are provided. In this study, the heat transfer coefficient in terms of the cost function is presented in the best case. The optimal values of solid volume fraction, nanoparticle's diameter and Reynolds number are provided to achieve the maximum heat transfer coefficient and minimum cost.

2. The NanoFluid's Multi-Objective Optimization

2.1. NSGA-II Algorithm:

In this study, the multi-objective optimization is executed by non-dominated sorting genetic algorithm II (NSGA-II) [26]. The advantages of NSGA-II over weighting method are a uniformly distributed Pareto-optimal front, suitable detecting Pareto-optimal front for non-convex two objective problems, avoiding time consuming and presenting the Pareto-optimal solutions in a single run only, in the NSGA-II. Also the disadvantages of epsilon-constraint method over NSGA-II are difficulty in choice of perfect value for ϵ vector, none equality-spaced Pareto solutions, requiring a large number of iterations like weighting method, in the epsilon-constraint method. Simulation results on some test problems show that the proposed NSGA-II, in most problems, is able to find so better spread of solutions and better convergence near the true Pareto-optimal front compared to Pareto archived evolution strategy (PAES) and strength Pareto evolutionary algorithm (SPEA) [26, 27].

This algorithm uses two functions of non-dominated sorting and crowding distance. In the non-dominated sorting function, all points are compared two by two. Then, each answer (point) is calculated as many times as dominated by other answers. After this process, a set of answers which is dominated by no other answers, has gained the first rate and has been put in the first front. Setting aside these points, the comparing operation is subsequently repeated until all answers are ranked in fronts. This subprogram takes population members as inputs, ranks them, and puts them into fronts in proportion to their ranks.

The crowding distance function is designed to avoid population members accumulating in a small distance and avoid the remained interval being blank. This function is utilized for comparison between members of a front which have equal ranks. For each reference point, the normalization

Euclidean distance of each solution of the front, compared to the previous and the next member and also the first and the last member of the population, is calculated according to Eq. (1) and Fig. 1. Normalization is used to avoid the problem that the objectives are in the different scale.

$$d^*_{ij} = \frac{\left|f_1^k - f_1^j\right|}{f_1^{max} - f_1^{min}} \, , d^*_{ik} = \frac{\left|f_2^k - f_2^j\right|}{f_2^{max} - f_2^{min}} \, , CD_i = d^*_{ij} + d^*_{ik} \quad (1)$$

First of all, N numbers of initial populations (Pt) are generated randomly. Then, objective function values are calculated for initial population and these members are ranked and their crowding distances are determined. Choosing parents based on the rank and CD scale via the binary tournament selection method, cross-over and mutation operators are applied on them. This new population (Qt) combines with the previous population and the sorting operation is repeated. Among the total available populations, which their members are also more than the initial population, N numbers of the population's upper members are selected for the other generation. Upper fronts are firstly selected to choose the population of the other generation and then if the number of population members gets more than N by selecting another front, choosing a sufficient number of that front is done according to the CD scale. The general trend of algorithm is shown in Fig. 2.

The NSGA-II flowchart has been shown in Fig. 3. As specified, the response surface method has been employed to determine the fitness functions in the optimization algorithm. As well, genetic operators include cross over and mutation are applied in order to generate a new population. Finally, the optimization process is wrapped up with condition of repetitions number.

2.1.1. Problem formulation

The NSGA-II algorithm has been used to reduce the cost and increase the heat transfer coefficient. For this purpose, three variables including solid volume fraction (φ), diameter of nanoparticles (Dp), and Reynolds number (Re) are intended as optimization variables.

The statement of the multi-objective optimization problem is as follows:

Minimize $f(y)$ and maximize $h(y)$

$$\text{Subject to } g_j(X) \le 0 \ \ for \ \ j = 1, n_c \qquad (2)$$

$$X_i^l \le X \le X_i^u$$

Which *f(y)* and *h(y)* are called objective function (cost and heat transfer coefficient) in GA; X determines design variables; g_j is a constraint; n_c represents the number of constraints; X_i^l and X_i^u are the lower band and upper band of the design variables, respectively.

Given that the NSGA-II algorithm uses the genetic algorithm to create the initial population and produce other generations, so cross-over and mutation operators are defined [28, 29]. The single point cross-over operator and the Gaussian mutation operator are applied in this section. Parameters of crossover percentage and mutation percentage are respectively set as 0.8 and 0.5; and mutation rate is set as 0.3. These values have been obtained with multiple runs of the optimization algorithms with different probability and different population size and compare the results.

Objective functions in the two-objective optimization are included the cost function and the heat transfer coefficient function. The cost evaluation function and the heat transfer coefficient can be achieved with the help of empirical data and using response surface method.

2.2. Approximation of objective functions

2.2.1. Response Surface Methodology

Response Surface Methodology (RSM) is a powerful tool for optimization in engineering problems. The approach is applicable when there are several variables that affect the efficiency of a system. The term of "response" implies the performance index of system where independent variables (or input variables) are adjusted by the operator. The focus of this research is the exploitation of RSM to develop a suitable correlation between input variables and the response. The correlation is based on the obtained data from the system. Consider the following correlation [25]:

$$y = \beta_0 + \beta_1 x_1 + \beta_2 x_2 + \varepsilon \qquad (3)$$

The above equation is a linear function of three unknown parameters i.e. β_0, β_1 and β_2. The independent variables x_1 and x_2 are commonly called predictor variables, and y is the target function.

To determine the regression coefficients of β in Eq. (3), least squares approach is utilized.

The matrix form of Eq. (3) can be written as:

$$Y = X\beta + \varepsilon \tag{4}$$

where Y is an n × 1 vector of the observations, X is an n × p matrix of the levels of the independent variables, β is a p × 1 vector of the regression coefficients, and ε is an n × 1 vector of random errors.

To gauge the precision of the linear regression model, several techniques are available such as properties of the Least Squares Estimators.

Least squares approach produces an unbiased estimator of the parameter β in the multiple linear regression models. The sum of squares of the residuals is defined as:

$$SS_E = \sum_{i=1}^{n} (y_i - \hat{y}_i)^2 = \sum_{i=1}^{n} e_i^2 = e^T e \tag{5}$$

where e_i is the difference between the measured value y_i and the exact value $\hat{y}_i$; the n×1 vector of residuals is denoted by:

$$e_i = y_i - \hat{y}_i \tag{6}$$

Because $X^T Xb = X^T y$, hence one may derive a computational formula for SS_E as:

$$SS_E = y^T y - b^T X^T y \tag{7}$$

Eq. (7) is called the error or residual sum of squares.

Unbiased estimator of σ^2 can be shown as:

$$\sigma^2 = \frac{SS_E}{n-p} \tag{8}$$

where n is the number of measurements and p represents the number of regression coefficients.

The total sum of squares is:

$$SS_T = y^T y - \frac{\left(\sum_{i=1}^{n} y_i\right)^2}{n} = \sum_{i=1}^{n} y_i^2 - \frac{\left(\sum_{i=1}^{n} y_i\right)^2}{n} \tag{9}$$

Then the coefficient of multiple determination R^2 is defined as

$$R^2 = 1 - \frac{SS_E}{SS_T} \tag{10}$$

R^2always rises as the number of terms in the model increases, so to avoid this issue it is preferred to use an adjusted R^2 as:

$$R_{adj}{}^2 = 1 - \frac{SS_E/(n-p)}{SS_T/(n-1)} = 1 - \frac{n-1}{n-p}(1-R^2) \quad (11)$$

In the next step, a cubic regression is utilized to assess the response variables achieved from the experiments so that the best fitting is obtained by the mathematical model. The accuracy of regression models were also tested by means of the analysis of variance (ANOVA).

For the flow of MgO/water nanofluid in a double tube heat exchanger, heat transfer coefficient data in terms of solid volume fraction, diameter of nanoparticle, and Reynolds number have been used to approximate the proper correlation by response surface method. The heat transfer coefficients data are for solid volume fractions in range of 0.5 to 2%, nanoparticle size in the range of 20nm to 60nm and Reynolds numbers between 2865 and 25760. Figure 4 shows a schematic of the experimental set-up along with the measured data given in Ref. [24].

2.2.2. Analysis of variance (ANOVA)

The statistical significance is evaluated for those cubic models by the ANOVA. The ANOVA results of the cubic model of the heat transfer coefficient are listed in Table 1. In the heat transfer coefficient model, the large value of the coefficient of multiple determination (R^2 = 0.9979). The large F-value is 7004 indicates the great significance of the regression model. The associated P-values less than 0.05 for the model indicate that the model terms are statistically significant and the effects of the model terms with the P-value greater than 0.05 are insignificant. All of the insignificant terms of the model have been eliminated.

Table 2 gives the ANOVA results of the cubic model of the standard deviation of cost. It is obvious that cost function has no relation by Re. So, the cost model has been presented in terms of φ and D_p. The cost regression model has a high value of goodness-of-fit (R^2 = 0.9973). This implies that only 0.27% of total variation cannot be reflected by the cubic model, which implies the model reflects the response variable accurately. The high F-value of 7605 and low P-value in regression model indicate the significance of the regression model.

2.2.3. Regression model of responses

The regression response surface models for evaluating the objective functions of heat transfer coefficient and cost are presented as:

$$h = -17.4 + 68.38\,\varphi + 0.44\,D_p + 0.01\,\mathrm{Re} - 0.11\,\varphi.D_p - 0.0003\,\varphi.D_p - 0 - 58.3\,\varphi^2 - 0.0049\,{D_p}^2 + 0.0009\,\varphi^2.Re + 15.7\,\varphi^3 \quad (12)$$

$$Cost = 21.56 - 90.88\,\varphi + 19.14\,D_p - 1.21\,\varphi.D_p + 38.46\,\varphi^2 - 0.56\,{D_p}^2 + 0.27\,\varphi^2.D_p - 18.3\,\varphi^3 + 0.004\,{D_p}^3 \quad (13)$$

The normal probability plots of the residuals for heat transfer coefficient and cost have been shown in Figs. 5(a) and 5(b), respectively.

Fig. 6 shows a comparison between predicted and experimental values of the response variable of heat transfer coefficient and cost by using resulted three-order polynomial equations. Results confirm that the experimental values are in good agreement with the predicted values.

The three-dimensional response surface graph of the cost in terms of two variables of the solid volume fraction and diameter of the nanoparticle is demonstrated in Fig. 7.

The three-dimensional response surface graph of the heat transfer coefficient in terms of the solid volume fraction, the diameter of the nanoparticle, and Reynolds numbers is presented. The heat transfer coefficient at solid volume fractions of 0.5, 1.25 and 2 is provided in Figs. 8. The heat transfer coefficient at Reynolds numbers of 2865, 14312 and 25760 is shown in Fig. 9, and finally the heat transfer coefficient at nanoparticle's diameters of 20nm, 40nm, and 60nm is displayed in Fig. 10. As observed in Figs. 8-10, the graphs tend to show relatively flat behavior except the graph that indicates the heat transfer coefficient variations versus volume fraction and particle diameter at low Reynolds number of 2865. This clearly unveils at low Reynolds numbers, the importance of optimization is more pronounced.

3. Results and Discussion

In several steps and at different values of the population members and the number of repetitions, the intended algorithm is executed in order to achieve the optimal result. The result of optimization, for the population of 50 members and repetition of 15 times, is presented in Fig. 11 as the terminating condition. Results in the first, the fifth, the tenth, and the Pareto front of optimization is presented in the figure to be compared the optimization process. These results are related to the

dominated and non-dominated fronts that the impact of dominated results elimination in each repetition is clearly recognizable. As obvious in the figure, values of optimum points in each optimizing generation is optimized compared to the previous generation and the best results have been finally presented. This trend indicates the performance rectitude of the optimization algorithm. The Pareto front curve is provided in the figure. Optimum points of the heat transfer coefficient and its equivalent cost can be obtained with the help of this curve. Considering the results, in order to reach the heat transfer coefficient of 280 W/m^{2}K, the cost is equal to 355$ per liter in the first generation, and 218$ per liter in the last generation which is in the Pareto front. This result proves that the optimization has been able to reduce the cost up to 38%.

The robustness of NSGA-II could be seen in Fig. 12. The curve fitted of the first, fifth, tenth, and the Pareto front of optimization is presented in the figure to be compared the optimization process. This shows that the further fronts are better in compare with previous fronts. The distance between any fronts is demonstrated by d1, d2, d3 and d4 in the figure.

Two-objective optimization's Pareto front for the heat transfer coefficient increment and the cost decrement is provided in Fig. 13. The last front of optimization is the Pareto front in which all points, compared to each other, are optimized and non-dominated. It can be concluded from the results that there will be about 10% of cost increment with the promotion of the heat transfer coefficient from 160 to 240 W/m^{2}K. Given the slight increase of the cost in this range, results of the first optimal zone can be utilized in industrial affairs. With increasing the heat transfer coefficient from 240 to 290 W/m^{2}K in the second range the expenses will be raised by 25%. Optimal results of this range can be used in experimental studies. The latest range of optimal results is related to particular utilizations of nanofluids. The cost increment in this section, due to the variation of heat transfer coefficient from 290 to 320 W/m^{2}K, is about 40%. As it is obvious in Fig. 13, if the cost function was the essential objective function, the first row in Table 3 is the best selection. Although for the optimum heat transfer coefficient, the second row in Table 3 is the best selection. The optimum values have been colored in the Table (rows 1 and 2).

Equation (14) is provided to achieve the optimal model of reaching the maximum heat transfer coefficient. It can be predicted by this Equation that how much the minimum required cost would be in terms of the specific heat transfer coefficient.

$$Cost = -\ 515.51 + 9.4648\,h - \ 0.045684\ \ h^2 \ + \ 0.000076\,h^3 \qquad (14)$$

One of the Pareto points is usually selected as a trade of point in the multi-objective optimization. In fact, the point of trade is a balance between the values of objective functions and in accordance with designer requirements and which objective function is more valuable for him, the designer can choose one of the Pareto front points. Unlike the weighting coefficients method, the Pareto optimization includes a set of optimal points that will be achieved by changing the coefficients. The optimal results in terms of each of variables of solid volume fraction, nanoparticle's diameter, and the Reynolds number are provided in Table 3. According to the amount of heat transfer coefficient, values of φ, Dp and Re with the lowest cost have been offered on the table.

As the results show, it is possible for the designer to select his optimal design through the provided results. The ultimate choice depends on the importance of each heat transfer coefficient and the cost functions for the designer and the selections can be replaced by each other. According to the results, the minimum cost is equal to \$336 per liter in terms of heat transfer coefficient of 320 W/m^2K, and it is equal to \$145 per liter in terms of heat transfer coefficient of 160 W/m^2K. The result reflects optimal costs respectively associated with the minimum and the maximum heat transfer coefficient.

4. Conclusion

Optimization of thermal systems has always motivated engineers and scholars because an optimized energy system presents many benefits such as reduction of operating costs, lowering harmful effects on environment, and saving in fossil energy sources. In the present work, the optimization of MgO-water nanofluids in order to increase the heat transfer coefficient and reduce the cost has been considered. In this optimization, response surface method is employed to determine the objective functions. To determine the objective functions, the heat transfer coefficient of nanofluids in terms of various values of solid volume fractions, diameters of nanoparticles and Reynolds numbers are specified by experiment. Using the heat transfer coefficient and the cost in terms of intended variables, the response surface and the correlation between the heat transfer coefficient and the cost have been obtained. The correlation has a high precision and a regression coefficient of over 0.997. Using determined objective functions, the multi-objective optimization is performed by NSGA-II. Pareto front results show that due to the cost increment, the maximum heat transfer coefficient is achieved in three zones. The results indicate that changing the heat transfer coefficient from 171 to 320 W/m^2K, the cost increases from 145\$ per liter to 336\$ per liter in the best case. Both the heat transfer coefficient's changes and

optimization results have shown that the cost has fallen about 38% in the best case compared to the first generation.

References:

[1] J. Eastman, S. U. S. Choi, S. Li, W. Yu, L. J. Thompson, and and L. J. Eastman, J.A., S.U.S. Choi, S. Li, W. Yu, "Anomalously increased effective thermal conductivities of ethylene glycol-based nanofluids containing copper nanoparticles," *Appl. Phys. Lett.*, vol. 78, no. 6, pp. 718– 720, 2001.

[2] S. U. S. Choi, Z. G. Zhang, W. Yu, F. E. Lockwood, and E. A. Grulke, "Anomalous thermal conductivity enhancement in nanotube suspensions," vol. 2252, no. 2001, pp. 15–18, 2009.

[3] M. Fakoor Pakdaman, M. a. A. Akhavan-Behabadi, and P. Razi, "An experimental investigation on thermo-physical properties and overall performance of MWCNT/heat transfer oil nanofluid flow inside vertical helically coiled tubes," *Exp. Therm. Fluid Sci.*, vol. 40, no. 25, pp. 103–111, Jul. 2012.

[4] P. Razi, M. a. Akhavan-Behabadi, M. Saeedinia, and M. a. Akhavan-Behabadi, "Pressure drop and thermal characteristics of CuO–base oil nanofluid laminar flow in flattened tubes under constant heat flux," *Int. Commun. Heat Mass Transf.*, vol. 38, no. 7, pp. 964–971, Aug. 2011.

[5] M. Hemmat Esfe, S. Saedodin, and M. Mahmoodi, "Experimental studies on the convective heat transfer performance and thermophysical properties of MgO-Water nanofluid under turbulent flow," *Exp. Therm. Fluid. Sci.*, vol. 52, pp. 68–78, Jan. 2013.

[6] M. Hemmat Esfe, S. Saedodin, O. Mahian, and S. Wongwises, "Thermophysical properties, heat transfer and pressure drop of COOH-functionalized multi walled carbon nanotubes/water nanofluids," *Int. Commun. Heat Mass Transf.*, vol. 58, pp. 176–183, Nov. 2014.

[7] M. Hemmat Esfe, S. Saedodin, O. Mahian, and S. Wongwises, "Heat transfer characteristics and pressure drop of COOH-functionalized DWCNTs / water nanofluid in turbulent flow at low concentrations," *Int. J. Heat Mass Transf.*, vol. 58, pp. 186–194, Jun.

2014.

[8] M. Hemmat Esfe, H. Rostamian, M. Afrand, A. Karimipour, and M. Hassani, "Modeling and estimation of thermal conductivity of MgO–water/EG (60:40) by artificial neural network and correlation," *Int. Commun. Heat Mass Transf.*, vol. 68, pp. 98–103, Nov. 2015.

[9] M. Hemmat Esfe, S. Saedodin, M. Bahiraei, D. Toghraie, O. Mahian, and S. Wongwises, "Thermal conductivity modeling of MgO/EG nanofluids using experimental data and artificial neural network," *J. Therm. Anal. Calorim.*, vol. 118, no. 1, pp. 287–294, 2014.

[10] M. Hemmat Esfe, S.Wongwises, A. Naderi, A. Asadi, M. R. Safaei, H. Rostamian, M. Dahari, "Thermal conductivity of Cu/TiO_2–water/EG hybrid nanofluid: Experimental data and modeling using artificial neural network and correlation," *Int. Commun. Heat Mass Transf.*, vol. 66, pp. 100–104, May 2015.

[11] M. Hemmat Esfe, S. Saedodin, A. Naderi, A. Alirezaie, A. Karimipour, S. Wongwises, M. Goodarzi, and M. bin Dahari, "Modeling of thermal conductivity of ZnO-EG using experimental data and ANN methods," *Int. Commun. Heat Mass Transf.*, vol. 63, pp. 35–40, Apr. 2015.

[12] S. khosrojerdi, M. Vakili, M. Yahyaei, and K. Kalhor, "Thermal conductivity modeling of graphene nanoplatelets/deionized water nanofluid by MLP neural network and theoretical modeling using experimental results," *Int. Commun. Heat Mass Transf.*, vol. 74, pp. 11–17, 2016.

[13] M. Hojjat, S. G. G. Etemad, R. Bagheri, and J. Thibault, "Thermal conductivity of non-Newtonian nanofluids : Experimental data and modeling using neural network," *Int. J. Heat Mass Transf.*, vol. 54, no. 5–6, pp. 1017–1023, Feb. 2011.

[14] M. Hemmat Esfe, S. Saedodin, N. Sina, and M. Afrand, "Designing an artificial neural network to predict thermal conductivity and dynamic viscosity of ferromagnetic nanofluid," *Int. Commun. Heat Mass Transf.*, vol. 68, pp. 50–57, Jun. 2015.

[15] N. Zhao, X. Wen, J. Yang, S. Li, and Z. Wang, "Modeling and prediction of viscosity of water-based nanofluids by radial basis function neural networks," *Powder Technol.*, vol. 281, pp. 173–183, Sep. 2015.

[16] F. Youse, H. Karimi, M. Mehdi, F. Yousefi, H. Karimi, and M. M. Papari, "Modeling viscosity of nanofluids using diffusional neural networks," *J. Mol. Liq.*, vol. 175, pp. 85–90, Nov. 2012.

[17] E. Heidari, M. A. Sobati, and S. Movahedirad, "Accurate prediction of nanofluid viscosity using a multilayer perceptron artificial neural network (MLP-ANN)," *Chemom. Intell. Lab. Syst.*, 2016.

[18] Y.-T. Yang, H.-W. Tang, B.-Y. Zeng, and C.-H. Wu, "Numerical simulation and optimization of turbulent nanofluids in a three-dimensional rectangular rib-grooved channel," *Int. Commun. Heat Mass Transf.*, vol. 66, pp. 71–79, Aug. 2015.

[19] F. A. Boyaghchi, M. Chavoshi, and V. Sabeti, "Optimization of a novel combined cooling, heating and power cycle driven by geothermal and solar energies using the water/CuO (copper oxide) nanofluid," *Energy*, vol. 91, pp. 685–699, Nov. 2015.

[20] H. Safikhani, A. Abbassi, A. Khalkhali, and M. Kalteh, "Multi-objective optimization of nanofluid flow in flat tubes using CFD, Artificial Neural Networks and genetic algorithms," *Adv. Powder Technol.*, vol. 25, no. 5, pp. 1608–1617, Sep. 2014.

[21] S. Halelfadl, A. M. Adham, N. Mohd-Ghazali, T. Maré, P. Estellé, and R. Ahmad, "Optimization of thermal performances and pressure drop of rectangular microchannel heat sink using aqueous carbon nanotubes based nanofluid," *Appl. Therm. Eng.*, vol. 62, no. 2, pp. 492–499, Jan. 2014.

[22] A. Mwesigye and Z. Huan, "Thermodynamic analysis and optimization of fully developed turbulent forced convection in a circular tube with water–Al_2O_3 nanofluid," *Int. J. Heat Mass Transf.*, vol. 89, pp. 694–706, Oct. 2015.

[23] P. Mohammad Zadeh, T. Sokhansefat, A. B. Kasaeian, F. Kowsary, and A. Akbarzadeh, "Hybrid optimization algorithm for thermal analysis in a solar parabolic trough collector based on nanofluid," *Energy*, vol. 82, pp. 857–864, Mar. 2015.

[24] M. Hemmat and E. Seyfolah, "Turbulent forced convection heat transfer and thermophysical properties of Mgo – water nanofluid with consideration of different nanoparticles diameter , an empirical study," pp. 1205–1213, 2015.

[25] R.H. Myers, D.C. Montgomery, C.M. Anderson-Cook, Response surface methodology: process and product optimization using designed experiment, third ed. Wiley, UK, 2009.

[26] K. Deb, A. Pratap, S. Agarwal, T. A. M. T. Meyarivan, "A fast and elitist multiobjective genetic algorithm: NSGA-II," IEEE transactions on evolutionary computation, 6(2), pp. 182–197, 2002.

[27] C. Sivapragasam, Multi-objective evolutionary techniques in defining optimal policies for real time operation of reservoir systems, Diss. PhD Thesis (National University of Singapore, Singapore), 2002.

[28] A.E. Eiben, S.K. Selmar, "Parameter tuning for configuring and analyzing evolutionary algorithms", Swarm and Evolutionary Computation, vol. 1, no. 1, pp. 19–31, Mar. 2011.

[29] A.R. Ghasemi, M.H. Hajmohammad, "Multi-objective optimization of laminated composite shells for minimum mass/cost and maximum buckling pressure with failure criteria under external hydrostatic pressure", Struct Multidisc Optim, vol. 55, no. 3, pp. 1051–1062, Aug. 2016.

Table 1: Analysis of variance (ANOVA) for heat transfer coefficient:

Source	DF	Adj SS	Adj MS	F	P
Model	11	764633	69512	7004	< 0.0001
φ	1	1688	1688	170	< 0.0001
D_P	1	13937	13937	1404	< 0.0001
Re	1	254033	254033	25595	< 0.0001
$\varphi . D_P$	1	155	155	16	0.0001
φ. Re	1	10953	10953	1104	< 0.0001
D_P. Re	1	2556	2556	258	< 0.0001
φ^2	1	2011	2011	203	< 0.0001
D_P^2	1	133	133	13	0.0003
Re^2	1	1411	1411	142	< 0.0001
φ^2. Re	1	464	464	47	< 0.0001
φ^3	1	305	305	31	< 0.0001
Residual error	164	1628	10		
Total	175	766261			

Standard deviation = 3.15

Predicted residual error of sum of squares (PRESS) =1895.17

R^2 (Adequate) = 99.79% R^2 (Predicted) =99.77% R^2 (Adjusted) =99.75%

Table 2: Analysis of variance (ANOVA) for heat transfer coefficient:

Source	DF	Adj SS	Adj MS	F	P
Model	8	720842	90105	7605	< 0.0001
φ	1	27689	27689	2337	< 0.0001
D_P	1	39154	39154	3305	< 0.0001
$\varphi . D_P$	1	3361	3361	284	< 0.0001
φ^2	1	4037	4037	341	< 0.0001
D_P^2	1	2246	2246	190	< 0.0001
$\varphi^2 . D_P$	1	177	177	15	0.0002
φ^3	1	416	416	35	< 0.0001
D_P^3	1	4623	4623	390	< 0.0001
Residual error	167	1979	12		
Total	175	722820			

Standard deviation = 3.44

Predicted residual error of sum of squares (PRESS) =2185.02

R^2 (Adequate) = 99.73% R^2 (Predicted) =99.71% R^2 (Adjusted) =99.70%

Table 3: Optimum points of the multi-objective optimization

φ	D_p (nm)	Re	Heat transfer coefficient	Cost
0.46	57	20151	160	145
1.82	35	30977	320	336
0.47	57	21903	171	146
0.95	51	31078	245	195
1.91	48	30924	312	272
1.35	53	34414	280	218
0.62	56	26706	203	156
1.82	41	31082	314	307
1.56	53	32525	285	234
1.22	53	31929	258	208
0.62	57	23478	185	156
0.83	54	32507	244	176
0.55	57	23197	181	151
1.35	56	32340	264	209
0.70	56	30174	226	164
0.71	56	27976	213	162
1.83	49	30897	302	263
0.74	54	31945	238	170
0.66	53	30992	232	167
0.63	56	27689	210	158
1.82	37	30977	318	328
1.82	39	31274	317	313
1.82	47	30989	304	270
1.59	49	33109	296	251
1.49	49	33109	289	245
0.57	57	23419	183	152
0.62	57	23478	184	155
1.50	49	33109	289	246
1.55	49	33109	293	249
1.55	49	33109	293	249
1.59	49	33109	296	251
1.82	35	30977	319	333
1.82	40	31069	314	308
1.82	36	30990	319	330
1.82	40	31286	316	310
1.82	40	31278	316	311
1.82	39	31282	317	313
1.82	36	30977	319	332

1.82	36	30977	319	332
0.46	57	20151	160	145

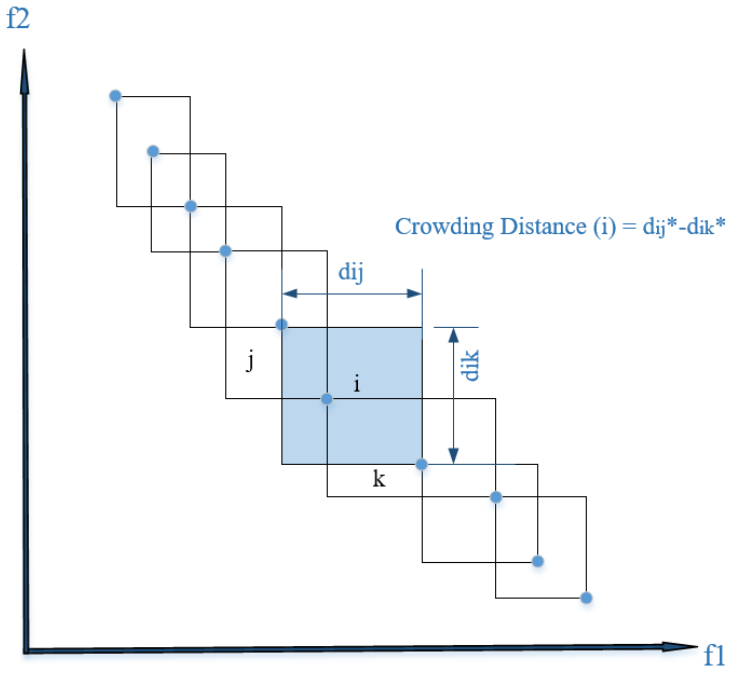

Fig. 1 Calculation of crowding distance in NSGA-II

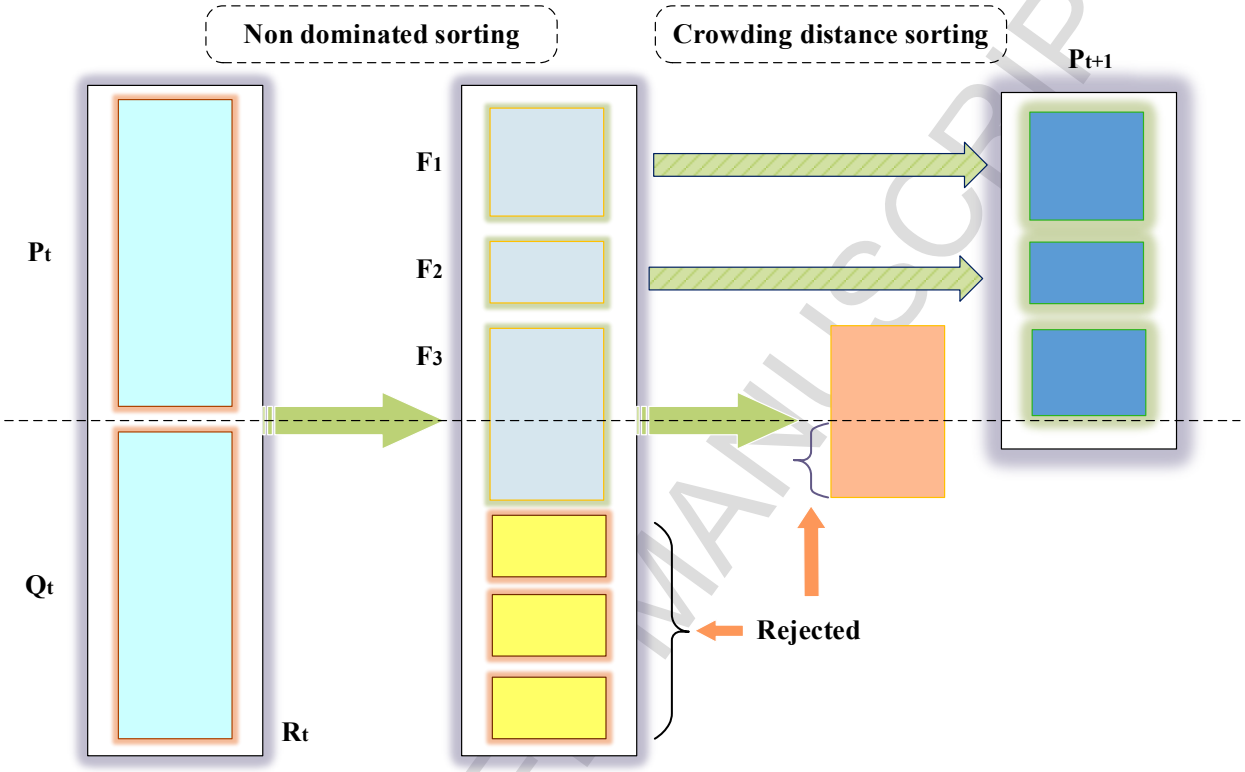

Fig. 2 Structure of NSGA-II

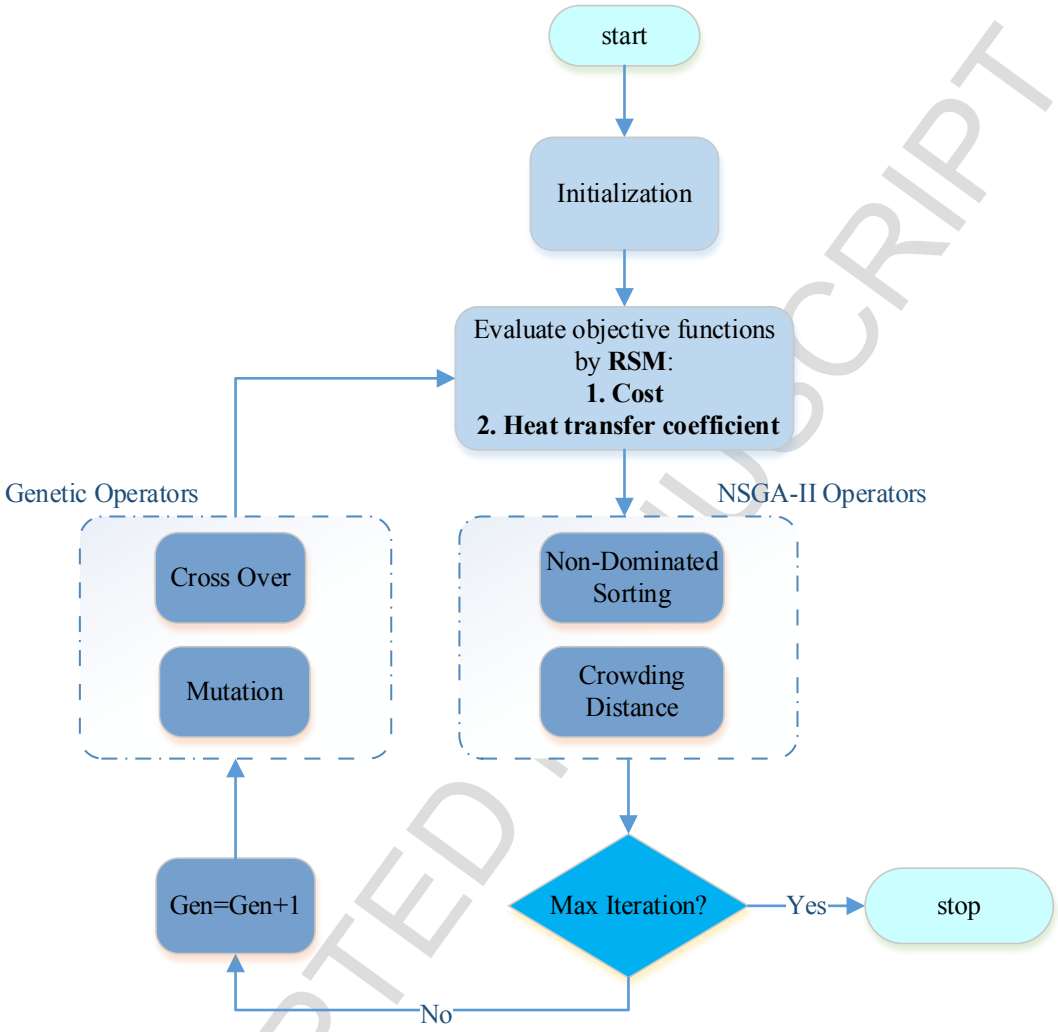

Fig. 3 Optimization flowchart

a)

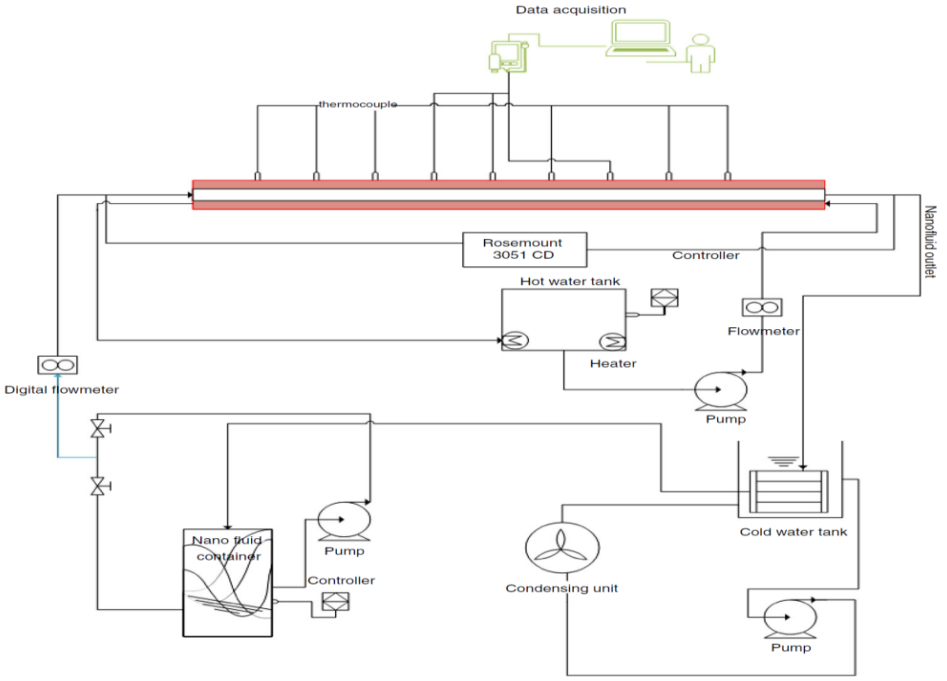
Data acquisition
thermocouple
Rosemount 3051 CD
Controller
Nanofluid outlet
Hot water tank
Flowmeter
Heater
Digital flowmeter
Pump
Cold water tank
Nano fluid container
Pump
Controller
Condensing unit
Pump

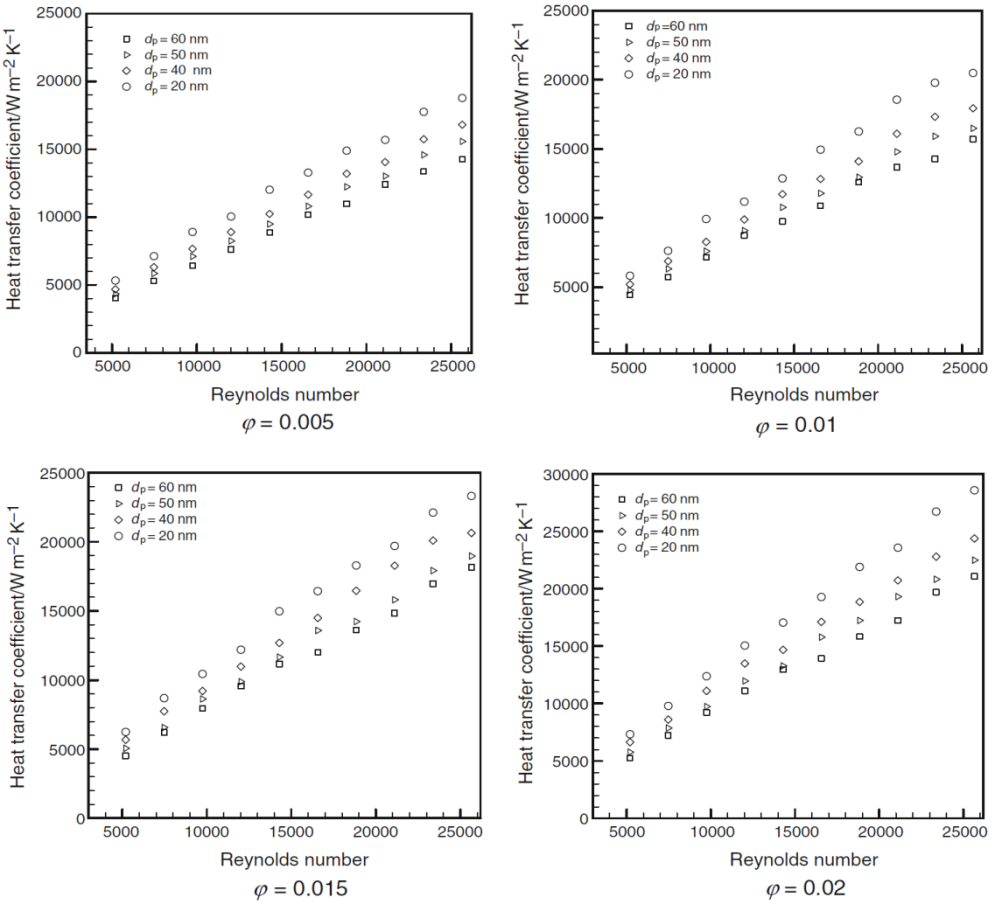
Heat transfer coefficient/W m−2 K−1
Reynolds number
dp = 60 nm
dp = 50 nm
dp = 40 nm
dp = 20 nm
φ = 0.005
φ = 0.01
φ = 0.015
φ = 0.02

b)

Fig. 4. (a) Experimental set-up for MgO/water nanofluid flow in double tube heat exchanger (b) heat transfer coefficients for various volume fractions of nanoparticles [24]

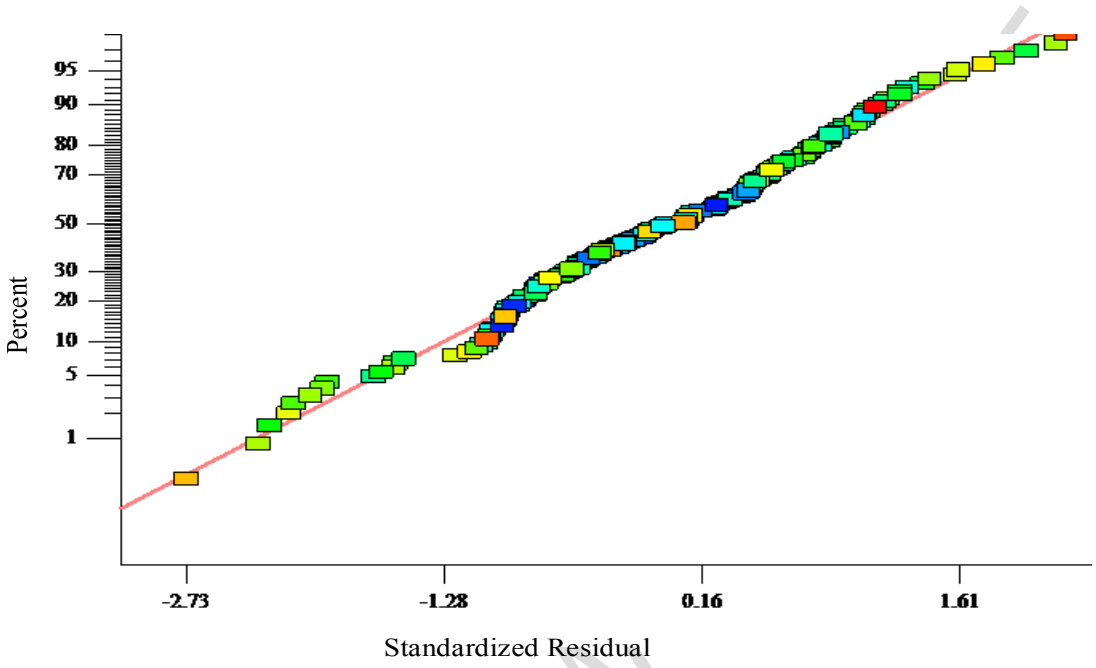

(a)

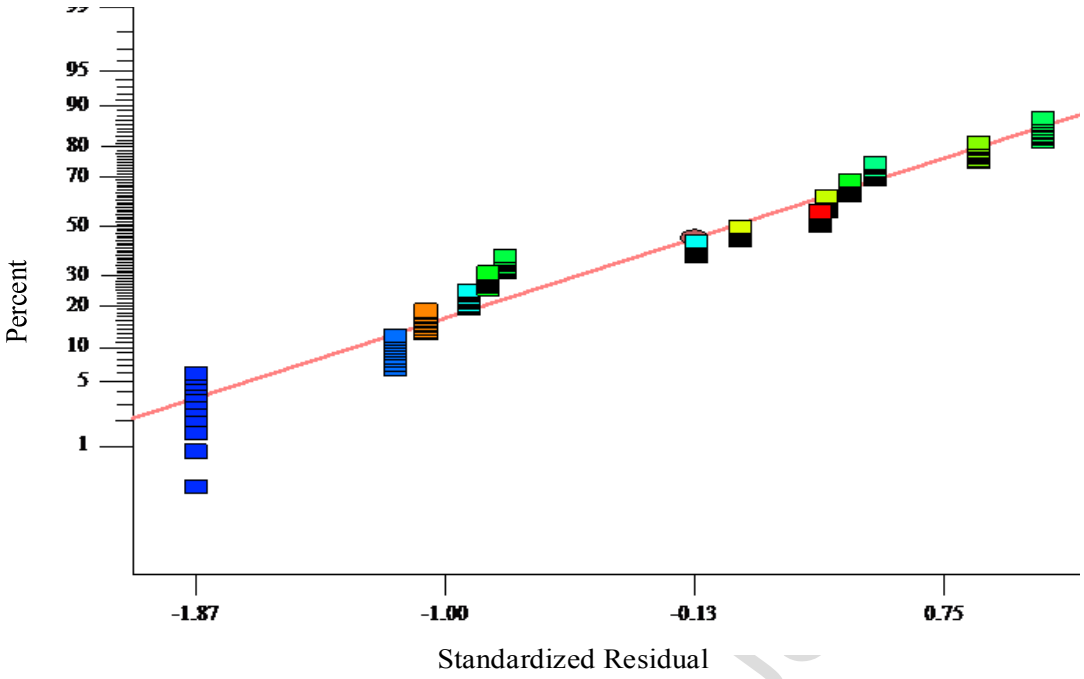

(b)

Fig. 5 Normal probability plot residuals. (a) heat transfer coefficient (b) Cost

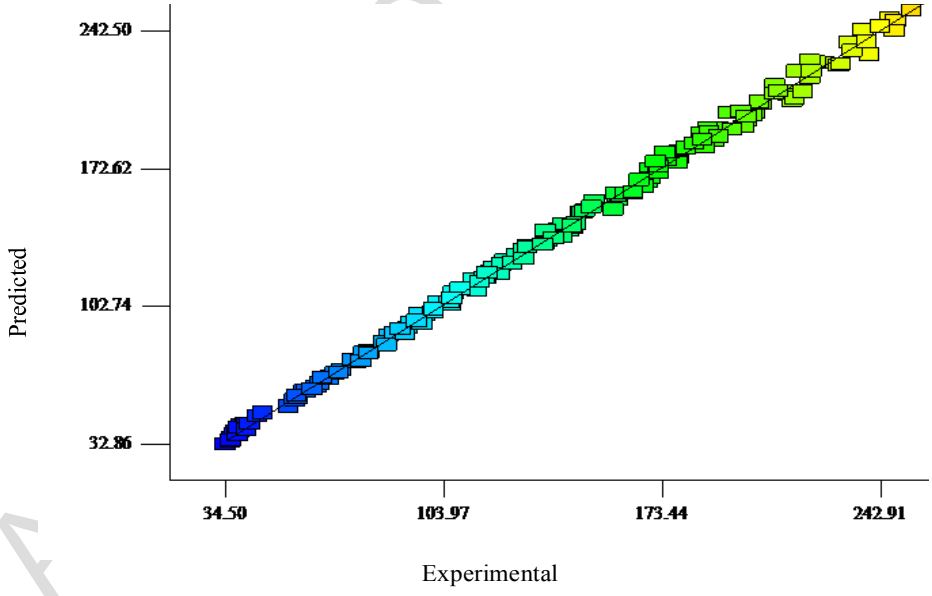

(a)

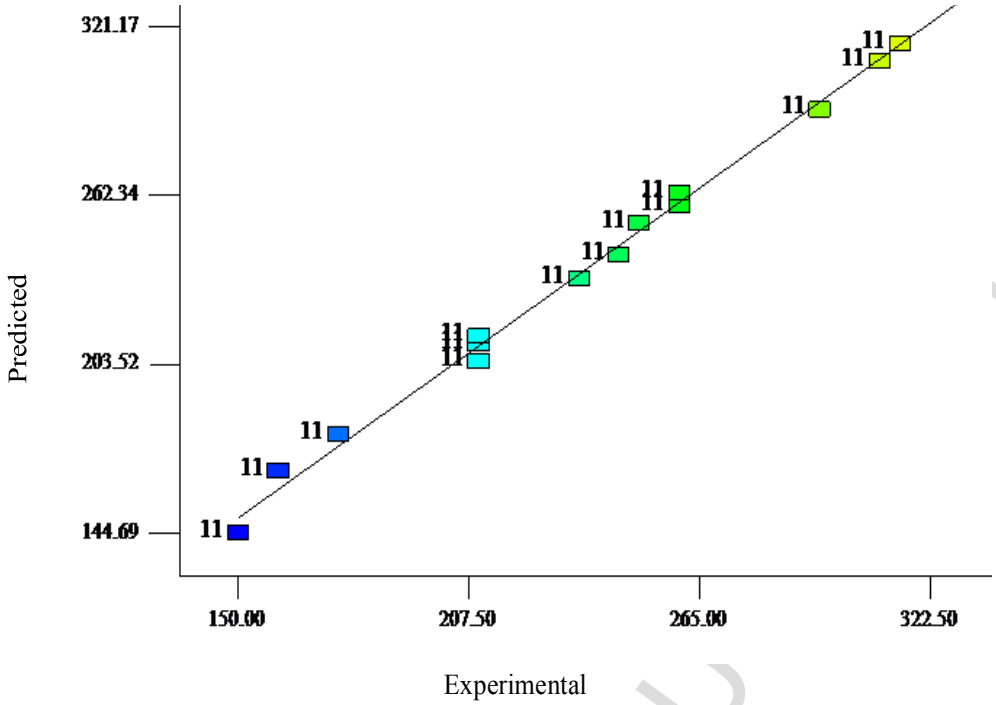

(b)

Fig. 6 Comparison of the experimental results and predicted values (a) *h* (b) *Cost*

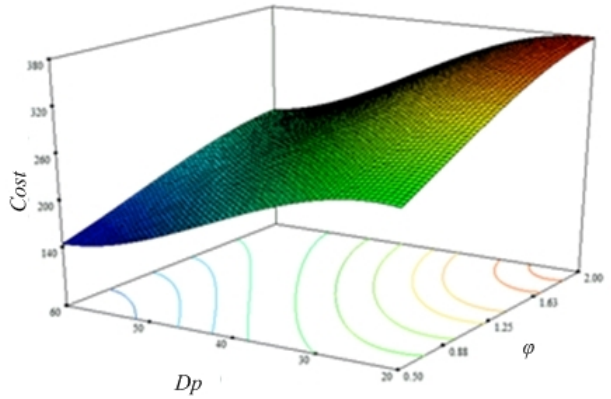

Fig. 7 Three-dimensional response surface graph of cost

a)

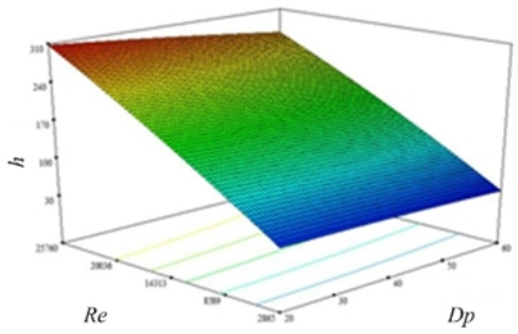

b)

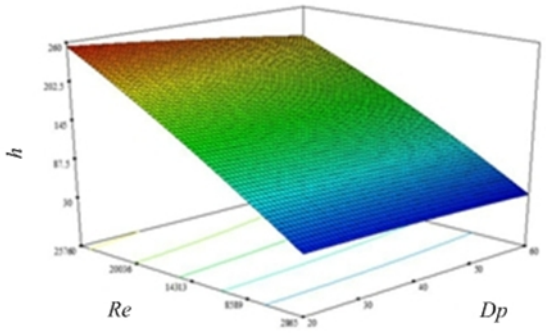

c)

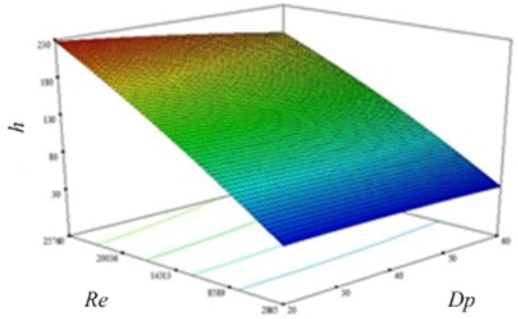

Fig.8 Three-dimensional response surface graphs of heat transfer coefficient for (*a*) φ =0.5, (b) φ=1.25, (c) φ=2

a)

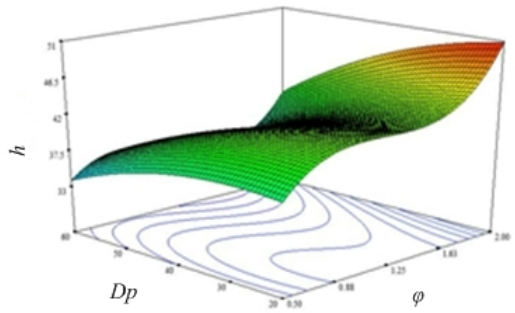

b)

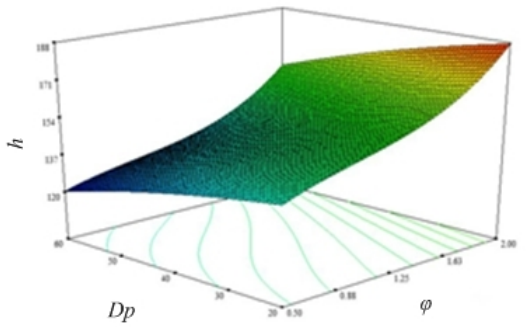

c)

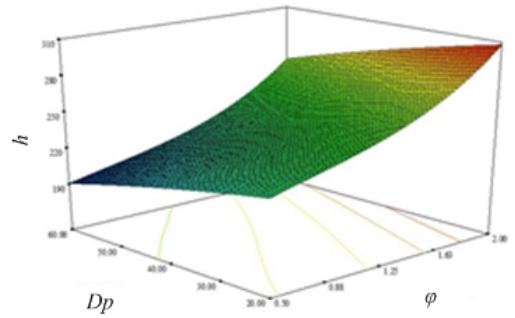

Fig.9 Three-dimensional response surface graphs of heat transfer coefficient for (*a*) Re = 2865, (b) Re = 14312, (c) Re = 25760

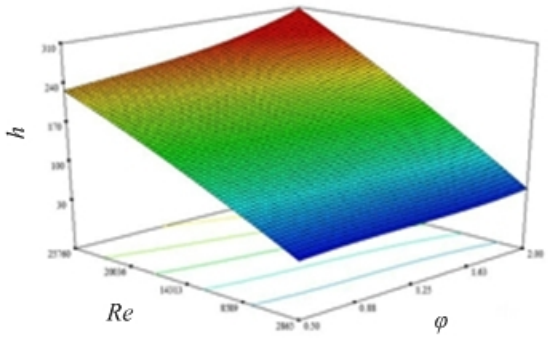

a)

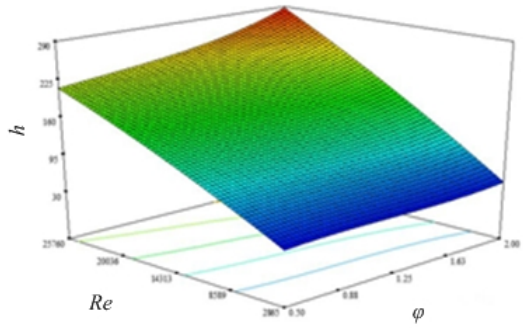

b)

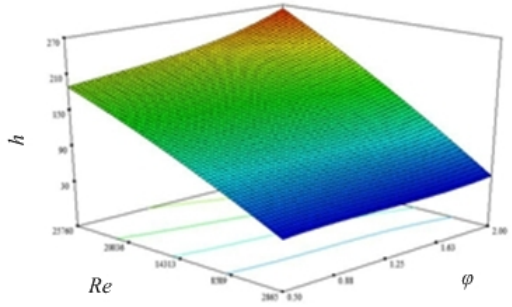

c)

Fig.10 Three-dimensional response surface graphs of heat transfer coefficient for (*a*) Dp = 20 nm, (b) Dp = 40 nm, (c) Dp = 60 nm

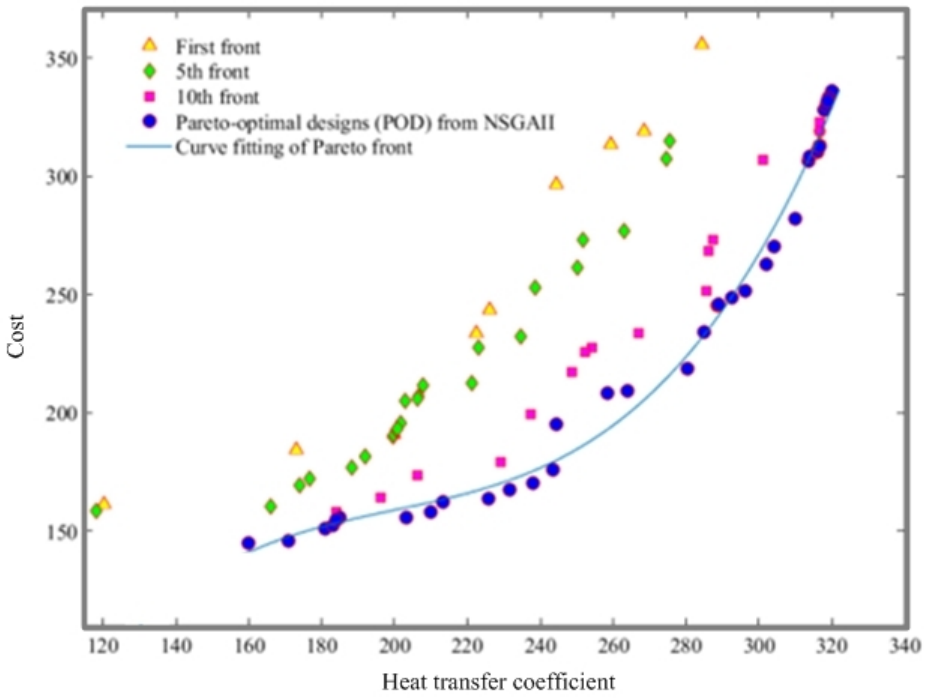

Fig. 11 Multi-objective optimization results by NSGA-II

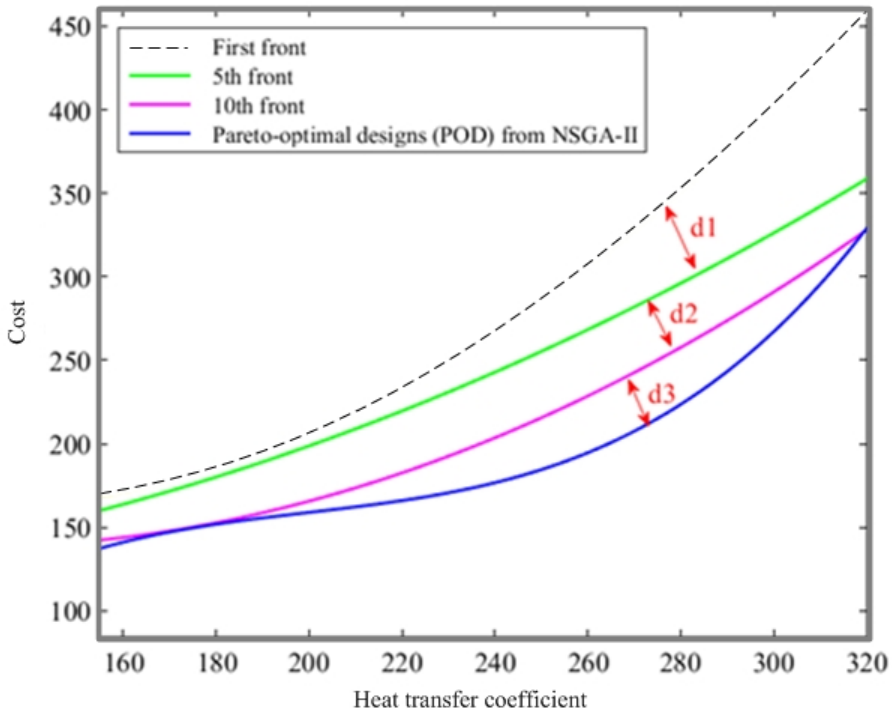

Fig. 12 Robust solutions obtained using NSGA-II

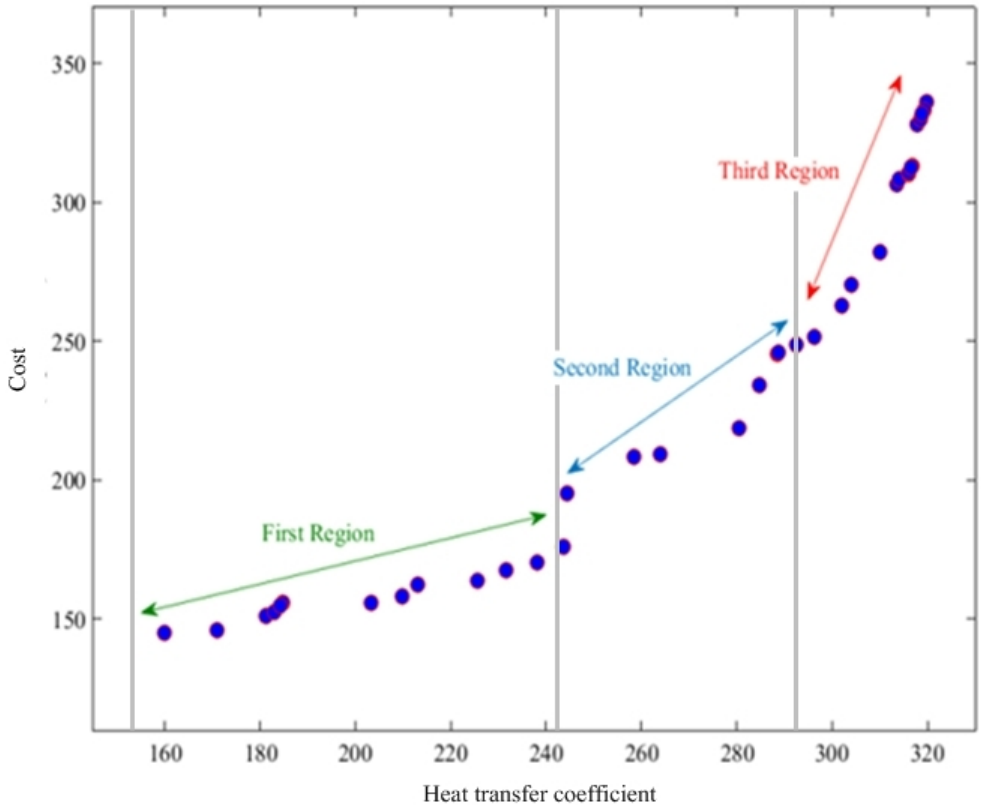

Fig. 13 Pareto optimal front

Highlights:

Multi-objective optimization of a double tube heat exchanger using nanofluids done.

Objective functions were heat transfer coefficient and cost.

Various sizes and volume fractions of particles as well as Reynolds number considered

A correlation is achieved to determine the optimal conditions